Article

Configuration Design and Kinematic Performance Analysis of a Novel Spatial 8R Hip Joint Rehabilitation Mechanism

Zengyu Jia, Ruiqin Li *, Yuan Wang, Juan Liu and Hailong Liang

School of Mechanical Engineering, North University of China, Taiyuan 030051, China
* Correspondence: liruiqin@nuc.edu.cn

Abstract: Lower limb movement disorders caused by various reasons are an important public health problem currently facing the world. To solve this problem, a novel spatial 8R mechanism with a stable structure and motion performance for human hip joint rehabilitation is proposed. Since the human body mainly performs coronal and sagittal plane movements, a spatial 8R mechanism with 2-DOF was designed to assist patients in rehabilitation training considering their actual circumstances. Based on the analysis of the Jacobian matrix and its condition number, the kinematics model and kinematics equation of the 8R mechanism in space were established. The mechanism has complete isotropic kinematics in single abduction and adduction, forward flexion and backward extension, and good dexterity and operability within the scope of the workspace; the correctness of the kinematics equation of the spatial 8R mechanism was verified by using the ADAMS software and theoretical calculation, and the regular variations of the mechanism's movement in one period under different motions were obtained. We concluded that the spatial 8R mechanism has a stable performance and can move smoothly.

Keywords: hip joint; spatial 8R mechanism; configuration design; kinematic model; manipulability

1. Introduction

Research on lower limb rehabilitation robots for patients with limb movement disorders is critical [1,2], with the design of rehabilitation mechanisms [3] representing a top priority in this field. Strengthening exercises with repetitive movements can help improve limb strength and functional recovery. However, traditional therapy is a long-term process that requires significant medical and human resources, the demand for which cannot be fully met due to the limited number of rehabilitation therapists. Recent research on robots has shown that rehabilitation robots can effectively assist patients in rehabilitation training [4]. Among these, wearable exoskeleton rehabilitation robots [5,6], which have many desirable characteristics, such as a simple structure, a light weight, portability, a low cost, safety and so on, have attracted increasing attention in rehabilitation training to assist patients.

The movements of the hip joint, knee joint and ankle joint are mainly involved in the movements of human lower limbs, with the hip joint playing the most important role [7]. The design of wearable exoskeleton hip rehabilitation mechanisms should take into account the range of motion and the volume of the mechanism itself. According to human biomechanics, assuming that the center of mass (The center of mass is referred to an imaginary point in the material system where mass is thought to be concentrated) is located in the pelvis, the width of the step and the moving position of the foot can be judged by the center of mass for each step [8–10]. The importance of the hip joint to human activities makes the design of the hip exoskeleton highly valued.

Patients have increasingly benefited with the advancement of rehabilitated exoskeletons, with various types of exoskeletons emerging [11,12]. Lee et al. [13] determined their potential for therapeutic or compensatory gait rehabilitation by studying how gait kinematics change with the application of virtual stiffness using hip exoskeleton robots. However,

research on adjusting limb kinematics according to the peripheral neuromechanics of the hip joint needs to be further explored and developed. Hsu et al. [14] designed a kinematically compatible 4-DOF robotic hip exoskeleton for gait rehabilitation, and verified the effect of this exoskeleton robot in assisting patients with rehabilitation training through the evaluation of dynamic assistance. Zhang et al. [15] designed an asymmetric fully constrained mechanism with three rotational degrees of freedom and three drives, and proposed the non-singular residue method based on reciprocity to eliminate singularities, thus preventing singularities. Along with the human hip joint, Zhang et al. [16] proposed a deformed mechanism with 3-UPS/S and 2-RPS/UPS/S configurations suitable for lower limb rehabilitation. The two configurations can be converted into each other, and the rotation center of the motion platform is designed to pass through the human hip joint to meet the needs of patients in different rehabilitation stages.

Because soft robots [17,18] are made of flexible materials, such as silicon, textiles, flexible plastics or cables, and because they are cheaper to manufacture, Miller-Jackson et al. [19] presented a hip flexion rehabilitation exoskeleton driven by a soft pneumatic actuator manufactured with flexible materials, and the target torque of hip flexion was evaluated, which verified the effectiveness of pneumatic muscles in providing hip flexion assistance. Because the structure and materials of soft robots are nonlinear and have multiple degrees of freedom, their action tasks are more complex than those of rigid robots, which require very high algorithm requirements [16,20,21] and need to be continuously developed. However, the selection of materials can provide a reference in the process of building experimental prototypes in subsequent mechanisms, and the rigid–flexible coupling [22–24] effect can make the rehabilitation training of patients more comfortable. Giovacchini et al. [25] proposed a lightweight active wearable power device with a carbon-fiber structure. Two elastic actuators were used to assist the flexion and extension of the hip joint. The dynamic characteristics of the actuator were experimentally characterized, and the effectiveness of the device in typical gait assistance scenarios was evaluated. This provides a reference direction for the development of rehabilitation robots. Designers of future rehabilitation devices should lay more emphasis on portability, intelligent control and modular structure design [26,27].

In view of the design of various hip joint rehabilitation devices, this paper proposes a new spatial 8R hip joint rehabilitation mechanism with a compact and stable structure, large stiffness, strong bearing capacity and simple control that fits closely on the hip joint and assists the thigh in forward flexion, backward extension, abduction and adduction movements. The rest of the paper is organized as follows. In Section 2, we introduce the configuration design of the spatial 8R mechanism. Then, in Section 3, we present the kinematic model of the spatial 8R mechanism and conduct kinematic performance analysis. Section 4 analyzes the variations in different movements in one cycle of this hip rehabilitation mechanism. Finally, conclusions are drawn in Section 5.

2. Configuration Design of the Spatial 8R Mechanism Configuration

The hip joint is stressed differently in different positions, and when standing, it is subjected to both gravity and abductor muscle tension. When standing and walking on one foot, because the center of gravity is connected to the femoral head on both sides, gravity exerts a torque effect on the joint, and the abductor muscles generate a reverse moment to maintain balance; furthermore, the proximal femur is subjected not only to compressive stress and tensile stress, but also to transverse circumferential stress and shear stress. When performing various movements, it is often necessary for the hip muscles to balance the weight, thus putting commensurate pressure on the hip joint. In this process, if the hip joint is used as the fulcrum, the force arm from the fulcrum to the center of gravity of the body is much greater than the force arm from the fulcrum to the hip muscles, and the strength of the hip muscles is much greater than the weight of the human body; thus, the joint force will be greater than the weight. Considering the biomechanics of the human hip joint, we have designed an improved hip rehabilitation mechanism that is suitable for

the human body and has a high degree of comfort. The spatial 8R mechanism has two degrees of freedom for rotation about the x axis and y axis. The device is an asymmetric mechanism composed of one static platform, two moving platforms, two 6R branch chains and two 2R constrained branch chains. The static platform is the hip exoskeleton in the hip rehabilitation mechanism, and the moving platform is the thigh exoskeleton, as shown in Figure 1.
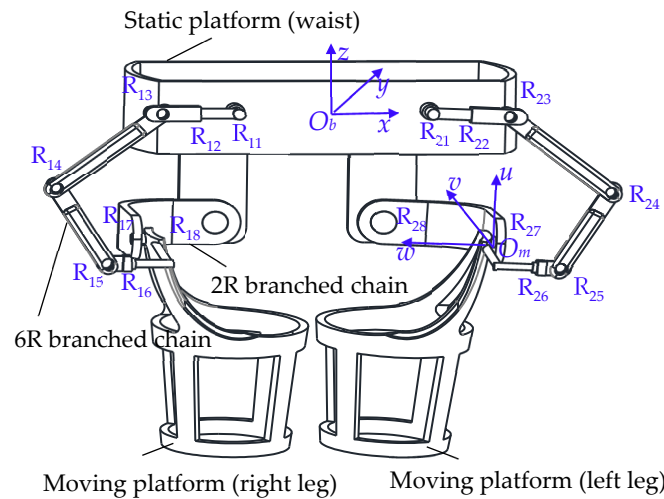
Figure 1. Model of hip joint rehabilitation mechanism and coordinate system.

Figure 1 shows the distribution positions of the eight revolute pairs of the 8R mechanism in this space. The axes of R_{11} and R_{18} are parallel to the Y axis of the static coordinate system, the axes of R_{12} and R_{16} are parallel to the X axis of the static coordinate system, and the axes positions of R_{13}, R_{14} and R_{15}, which are not described in detail, are clear. The mechanism is symmetrical from left to right, and the arrangement of the revolute pairs on one side is described as follows. The static coordinate system O_b-xyz and the moving coordinate system O_m-uvw are established on the static and moving platforms of the mechanism, as shown in the figure. The origin O_b of the static coordinate system is at the midpoint of revolute pairs R_{11} and R_{21}. The x-axis direction is the same as the O_bR_{21} direction, while the y-axis direction is perpendicular to $R_{11}R_{21}$ inward, and the z-axis direction is perpendicular upward. The origin om of the moving coordinate system is at the rotation center of the revolute pair R_{27}. The axis of the vertical revolute pair R_{27} faces up in the direction of the u axis, the axis of the vertical revolute pair R_{27} is inward in the direction of the v axis, and the direction of the w axis is left along the axis of the revolute pair R_{27}. The branch chain coordinate system R_{1i}-$x_{1i}y_{1i}z_{1i}$ (i = 1, 8) is established at the rotation center of the revolute pair R_{1i}. x-axis direction of the branch chain coordinate system. R_{11}-$x_{11}y_{11}z_{11}$ is oriented along the R_{11} axis, the y_{11} axis is oriented to the left along the connecting direction of $R_{11}R_{12}$, and the z_{11} axis faces vertically downward.

The moving platform and the static platform are designed as retractable components considering the actual circumstances of patients. The dimensions of each link are only given for the right side of the overall mechanism, and the distance between the two links is the distance between the centers of the revolute joints. The length of each link is as follows:

$R_{21}R_{22}$ = 47 mm; $R_{22}R_{23}$ = 45 mm; $R_{23}R_{24}$ = 160 mm; $R_{24}R_{25}$ = 120 mm; $R_{25}R_{26}$ = 33 mm; $^1R_{27}R_{28}$ = 172 mm; $^2R_{27}R_{28}$ = 127 mm.

The labeled numbers in the upper left corner of R represent the two dimension values of $R_{27}R_{28}$.

The hip rehabilitation mechanism is symmetrical from left to right. Taking the left-moving platform as an example, for the mechanism with few degrees of freedom, each branch chain will exert a constraint effect on the moving platform; thus, all the constraints loaded on the moving platform are the result of the joint action of all the constraint force

systems. Due to the joint constraints of the 6R and 2R branches, the mechanism cannot move along the x axis, y axis or z axis or rotate around the z axis, but can rotate around the x axis and y axis to carry out forward flexion and extension, abduction and adduction of the hip, respectively.

Suppose the kinematic spiral system of the fixed kinematic pair R_{11}, 5R branch chain, is

$$
\begin{cases}
\$_{12} = (0\ 1\ 0\ 0\ 0\ 0) \\
\$_{13} = (\cos\beta\ 0\ \sin\beta\ y_{13}\sin\beta\ z_{13}\cos\beta - x_{13}\sin\beta\ y_{13}\cos\beta) \\
\$_{14} = (\cos\beta\ 0\ \sin\beta\ y_{14}\sin\beta\ z_{14}\cos\beta - x_{14}\sin\beta\ y_{14}\cos\beta) \\
\$_{15} = (\cos\beta\ 0\ \sin\beta\ y_{15}\sin\beta\ z_{15}\cos\beta - x_{15}\sin\beta\ y_{15}\cos\beta) \\
\$_{16} = (0\ 1\ 0\ z_{16}\ 0\ x_{16})
\end{cases}
\tag{1}
$$

The motion of the 5R branch chain is an antihelix:

$$
\$^r = (0\ 0\ 0\ \sin\beta\ 0 - \cos\beta)
\tag{2}
$$

Equation (2) represents the antihelix of the 5R branch chain, and its physical meaning is as follows: The 5R branch chain is constrained by coupling motion around the x-axis and z-axis directions. By the joint constraint of the 5R branch chain and 2R branch chain, the moving platform can achieve forward flexion and backward extension around the y axis, but cannot rotate around the x axis. Therefore, the revolute pair R_{11} can control the motion of the mechanism around the x axis. R_{11} of the 6R branch chain is thus used as the drive, and the drive is installed at R_{17} of the 2R branch chain, so the mechanism will carry out decoupled motion around the x axis and y axis.

3. Kinematic Performance Analysis of the Spatial 8R Mechanism

To better verify the spatial 8R mechanism has good motion performance [28,29] and avoid unreasonable errors in the design of the mechanism, which could cause injuries when assisting patients in rehabilitation training, kinematic position analysis, dexterity analysis, maneuverability analysis and singularity analysis of the mechanism were carried out to ensure that the mechanism has improved motion characteristics.

3.1. Forward/Inverse Kinematics

The D-H method was used to analyze the kinematics and position of the mechanism. This method establishes the object coordinate system (also known as the link coordinate system) at each joint of the robot, thus determining the pose matrix (homogeneous transformation matrix) between adjacent links, and finally reflects the pose relationship between the end and the base through the results of continuous transformation. Additionally, the branch chain coordinate system R_{2i}-$x_{2i}z_{2i}$ (i = 1~8) was established at the rotation center of the revolute pair R_{2i}. The direction of each branch chain coordinate system is shown in Figure 2, where the coordinate system at R_{22} is the same as that at R_{26}, and the coordinate system at R_{25} and R_{21}, and z axis of R_{23} and R_{24}, is the same as that at R_{21}. The coordinate system R_{27}-$x_{27}z_{27}$ coincides with the moving coordinate system O_m-uvw. The D-H parameters of the 6R and 2R branches are shown in Tables 1 and 2.
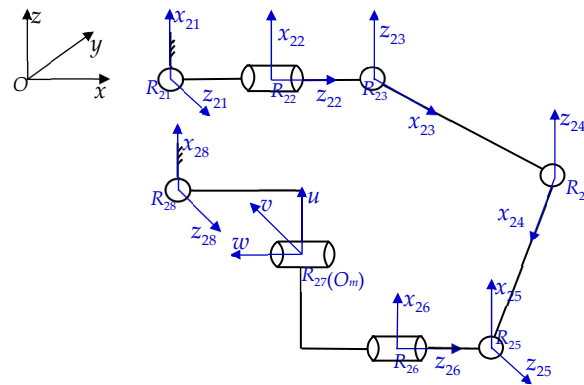
Figure 2. Limb coordinate systems.

Table 1. D-H parameters of 6R limb.

i	$\alpha_{i-1}/(°)$	a_{i-1}/mm	$\theta_i/(°)$	d_i/mm
1	90	g	θ_1	0
2	90	0	θ_2	l_1
3	90	0	θ_3	0
4	0	h	θ_4	0
5	0	m	θ_5	0
6	90	0	θ_6	l_2

Table 2. D-H parameters of 2R limb.

i	$\alpha_{i-1}/(°)$	a_{i-1}/mm	$\theta_i/(°)$	d_i/mm
1	90	k	θ_7	0
2	90	0	θ_8	l_3

In Tables 1 and 2, α_{i-1} is the rotation degree from z_{i-1} to z_i around the x_{i-1} axis. a_{i-1} is the distance from z_{i-1} to z_i along the x_i axis. θ_i is the rotation degree from x_{i-1} to x_i around the z_i axis. d_i is the distance from x_{i-1} to x_i along the z_i axis. g, m, n, k, l_1, l_2 and l_3 are constants, and θ_1, θ_2, θ_3, θ_4, θ_5, θ_6, θ_7 and θ_8 are variables.

The general formula of matrix transformation between two adjacent coordinate systems, $\{i\}$ and $\{i-1\}$, is:

$$
{}_{i}^{i-1}T = \begin{bmatrix} c\theta_i & -s\theta_i & 0 & a_{i-1} \\ s\theta_i c\alpha_{i-1} & c\theta_i c\alpha_{i-1} & -s\alpha_{i-1} & -d_i s\alpha_{i-1} \\ s\theta_i s\alpha_{i-1} & c\theta_i s\alpha_{i-1} & c\alpha_{i-1} & d_i c\alpha_{i-1} \\ 0 & 0 & 0 & 1 \end{bmatrix}
\tag{3}
$$

where s stands for sin and c stands for cos, the same as below.

Then, based on the D-H parameters of the 6R branch chain in Table 1 and Equation (3), we can obtain the transformation matrix of each revolute pair of the 6R branch chain.

For the 6R branch chain, the transformation matrix of each link is multiplied, and the transformation matrix of the 6R branch chain is obtained as follows:

$$
{}_{6}^{0}T1 = {}_{1}^{0}T {}_{2}^{1}T {}_{3}^{2}T {}_{4}^{3}T {}_{5}^{4}T {}_{6}^{5}T
\tag{4}
$$

Since joint 3 and joint 4 are parallel to each other,

$$
{}_{4}^{2}T1 = {}_{3}^{2}T {}_{4}^{3}T = \begin{bmatrix} c_{34} & -s_{34} & 0 & hc_3 \\ 0 & 0 & -1 & 0 \\ s_{34} & c_{34} & 0 & hs_3 \\ 0 & 0 & 0 & 1 \end{bmatrix}
\tag{5}
$$

where s_i stands for $\sin(\theta_i)$, c_i stands for $\cos(\theta_i)$, c_{ij} stands for $\cos(\theta_i + \theta_j)$, and s_{ij} stands for $\sin(\theta_i + \theta_j)$, the same as below.

Finally, the transformation matrix of the 6R branch chain is obtained:

$$
{}^0_6T_1 = \begin{bmatrix} n_x & r_x & t_x & p_x \\ n_y & r_y & t_y & p_y \\ n_z & r_z & t_z & p_z \\ 0 & 0 & 0 & 1 \end{bmatrix} \tag{6}
$$

where

$n_x = c_1 c_2 (c_{34} c_5 c_6 - s_{34} c_6 s_5) - s_1 (c_{34} c_6 s_5 + s_{34} c_5 c_6) + c_1 s_2 s_6$

$n_y = c_2 s_6 - (c_{34} c_5 c_6 - s_{34} c_6 s_5)$

$n_z = -c_1 (c_{34} c_6 s_5 + s_{34} c_5 c_6) - c_2 s_1 (c_{34} c_5 c_6 - s_{34} c_6 s_5) - s_1 s_2 s_6$

$r_x = s_1 (c_{34} s_5 s_6 + s_{34} c_5 s_6) - c_1 c_2 (c_{34} c_5 s_6 - s_{34} s_5 s_6) + c_1 c_6 s_2$

$r_y = s_2 (c_{34} c_5 s_6 - s_{34} s_5 s_6) + c_2 c_6$

$r_z = c_1 (c_{34} s_5 s_6 + s_{34} c_5 s_6) + c_2 s_1 (c_{34} c_5 s_6 - s_{34} s_5 s_6) - c_6 s_1 s_2$

$t_x = s_1 (c_{34} c_5 - s_{34} s_5) + c_1 c_2 (c_{34} s_5 + s_{34} c_5)$

$t_y = -s_2 (c_{34} s_5 + s_{34} c_5)$

$t_z = c_1 (c_{34} c_5 - s_{34} s_5) - c_2 s_1 (c_{34} s_5 + s_{34} c_5)$

$p_x = g - s_1 [s_{34}(m + l_2 s_5) + h s_3 - l_2 c_{34} c_5] - l_1 s_1 + c_1 c_2 [c_{34}(m + l_2 s_5) + h c_3 + l_2 s_{34} c_5]$

$p_y = -s_2 [c_{34}(m + l_2 s_5) + h c_3 + l_2 s_{34} c_5]$

$p_z = -c_1 [s_{34}(m + l_2 s_5) + h s_3 - l_2 c_{34} c_5] - l_1 c_1 - c_2 s_1 [c_{34}(m + l_2 s_5) + h c_3 + l_2 s_{34} c_5]$

Equation (6) is the pose of the terminal link coordinate system R_{26}-$x_{26}z_{26}$ relative to the static coordinate system O_b-xyz, which is the basic equation for kinematic analysis of 6R branch chains.

To verify the obtained results, the value of the 6R branch chain transformation matrix was calculated when $\theta_1 = \theta_2 = \theta_3 = 0°$, $\theta_4 = 90°$, $\theta_5 = 90°$ and $\theta_6 = 0°$, and the calculation result is

$$
{}^0_6T_1 = \begin{bmatrix} 1 & 0 & 0 & g - h \\ 0 & 1 & 0 & h \\ 0 & 0 & 1 & l_2 - m - l_1 \\ 0 & 0 & 0 & 1 \end{bmatrix} \tag{7}
$$

The calculation results show that the obtained ${}^0_6T_1$ is correct.

According to the D-H parameters of the 2R branch chain in Table 2 and Equation (3), we can obtain the transformation matrix of each revolute pair of the 2R branch chain.

For the 2R branch chain, the transformation matrix of each link is multiplied, and the transformation matrix of the 2R branch chain is:

$$
{}^0_2T_2 = {}^0_1T {}^1_2T = \begin{bmatrix} c_7 c_8 & -c_7 s_8 & s_7 & k - l_3 s_7 \\ s_8 & c_8 & 0 & 0 \\ -c_8 s_7 & s_7 s_8 & c_7 & -c_7 l_3 \\ 0 & 0 & 0 & 1 \end{bmatrix} \tag{8}
$$

By substituting $\theta_7 = \theta_8 = 0°$ into ${}^0_2T_2$, we can verify that it is correct.

In conclusion, the basic equations for the kinematic analysis of the 8R mechanism in this space are obtained. The pose matrix of the moving platform is expressed by the *Z-Y-X* Euler angle (α, β, γ):

$$
\mathbf{T} = \begin{bmatrix} c\alpha c\beta & c\alpha s\beta s\gamma - s\alpha c\gamma & c\alpha s\beta c\gamma + s\alpha c\gamma & x \\ s\alpha c\beta & s\alpha s\beta s\gamma + c\alpha c\gamma & s\alpha s\beta c\gamma - c\alpha s\gamma & y \\ -s\beta & c\beta s\gamma & c\beta c\gamma & z \\ 0 & 0 & 0 & 1 \end{bmatrix} \tag{9}
$$

where s_i stands for $\sin(\theta_i)$, c_i stands for $\cos(\theta_i)$, $\mathbf{T}$ is the pose matrix, (x, y, z) is the position coordinates of the origin O_m of the moving coordinate system in the static coordinate

system O_b-XYZ, and α, β and γ are the rotation angles of the moving platform around the OZ axis, OY axis and OX axis in the static coordinate system, respectively.

$$\begin{cases} {}^0_6T_1 = T \\ {}^0_2T_2 = T \end{cases} \tag{10}$$

It is known that R_{21} can control the rotation of the mechanism around the x axis, and a drive is installed at R_{21}, so the rotation angle of R_{21} around the x axis is equal to that of the moving platform. Moreover, the moving platform is concentrically matched with the revolute pair R_{27}, and its rotation angle around the y axis is equal to that of R_{27}.

The pose of the moving platform can be determined by the rotation angles θ_{21} and θ_{27} of R_{21} and R_{27} (corresponding to the angles θ_1 and θ_7 in the D-H parameter in Table 2).

$$\begin{cases} \theta_1 = \gamma \\ \theta_7 = \arccos(t) \end{cases} \tag{11}$$

where $t = \sin\beta\cos\gamma$.

This is the inverse position solution of the mechanism.

The position forward solution of the mechanism can be expressed as:

$$\begin{cases} \gamma = \theta_1 \\ \beta = \arcsin\left(\frac{\cos\theta_7}{\cos\theta_1}\right) \end{cases} \tag{12}$$

3.2. Velocity Jacobian Matrix and Dexterity Analysis of the Spatial 8R Mechanism

When the determinant of the Jacobian matrix of the mechanism is zero or tends toward infinity, the mechanism is rigid or has excess degrees of freedom. The mechanism should be far away from the singular configuration region. Through the analysis of the dexterity of the mechanism, the distortion degree of this motion can be measured quantitatively [30–32].

By differential operation on Equation (11), the velocity relation between the input and output of the mechanism can be expressed as

$$\begin{cases} \dot\theta_1 = \dot\gamma \\ \dot\theta_7 = -\frac{\dot\beta\cos\beta\cos\gamma - \dot\gamma\sin\beta\sin\gamma}{\sqrt{1-t^2}} \end{cases} \tag{13}$$

Equation (13) can be rewritten as follows.

$$\begin{pmatrix} \dot\theta_1 & \dot\theta_7 \end{pmatrix}^{\mathrm{T}} = J \begin{pmatrix} \dot\beta & \dot\gamma \end{pmatrix}^{\mathrm{T}} \tag{14}$$

where J is the velocity Jacobian matrix of the mechanism, which represents the linear transformation relationship between the output velocity of the moving platform and the driving velocity.

The Jacobian matrix J in Equation (14) is calculated as follows:

$$J = \begin{bmatrix} 0 & 1 \\ A_{21} & A_{22} \end{bmatrix} \tag{15}$$

where

$$A_{21} = -\frac{\cos\beta\cos\gamma}{\sqrt{1-t^2}}, \ A_{22} = \frac{\sin\beta\sin\gamma}{\sqrt{1-t^2}}$$

According to Equation (15), the condition number of the Jacobian velocity of the mechanism is calculated as

$$\begin{cases} \lambda_1 = 1 \\ \lambda_2 = -\frac{\cos\beta\cos\gamma}{\sqrt{1-t^2}} \end{cases} \tag{16}$$

According to the Jacobian condition number of the obtained velocity, when $\lambda_1 = 1$, the mechanism has a single abduction and adduction movement, indicating that the mechanism has good dexterity in this movement and has completely isotropic kinematics.

When $\theta_1 = \gamma = 0$, $\lambda_2 = -1$, the mechanism carries out a single forward flexion and backward extension movement, indicating that the kinematics of the mechanism are completely isotropic. Therefore, the spatial 8R mechanism has complete isotropy under a single motion and good dexterity during movement.

3.3. Manipulability Analysis of the Spatial 8R Mechanism

The manipulability ω of the mechanism ω is used to describe the comprehensive motion and overall flexibility of the mechanism in all directions. The determinant of the product of the Jacobian matrix and its transpose matrix can be defined as the metric index of robot manipulability, which is

$$\omega = \sqrt{\det(JJ^{\mathrm{T}})} \tag{17}$$

Further, the manipulability ω of this mechanism can be obtained as

$$\omega = \sqrt{\det(JJ^{\mathrm{T}})} = |\lambda_2| = \left| \frac{\cos\beta\cos\gamma}{\sqrt{1-t^2}} \right| \tag{18}$$

The distribution of ω in the workspace of $-90°\sim90°$ is show in Figure 3.
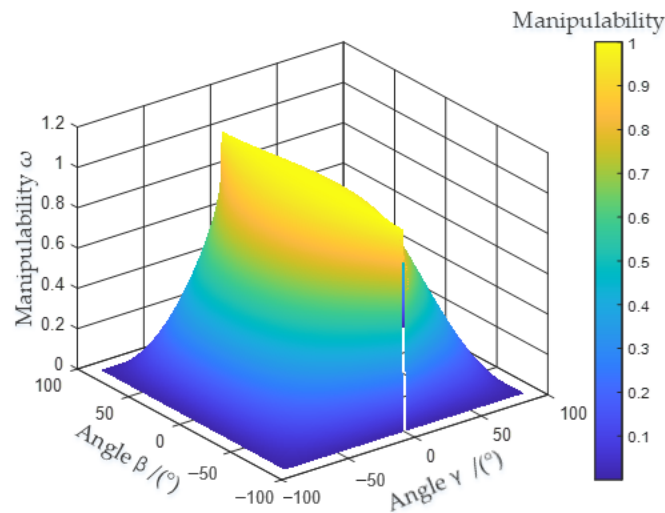
Figure 3. The distribution of ω values in $-90°\sim90°$.

As seen in Figure 3, the manipulability degree of (γ, β) near the points $(-90°, -90°)$, $(-90°, 90°)$, $(90°, -90°)$ and $(90°, 90°)$ approaches 0, and the value of ω near $(0, \beta_i)$ approaches infinity; thus, these positions are the singular configuration of the mechanism, where β_i represents the coordinate position on the β axis.

Table 3 shows the extreme motion angles of abduction and adduction, forward flexion and backward extension of the hip joint during the walking gait, corresponding to the motion ranges of γ and β.

Table 3. Hip joint range of motion.

Motion Type	Range of Motion/(°)
Flexion	0~125°
Extension	0~30°
Adduction	0~60°
Abduction	0~40°

According to Table 3, the boundary conditions of the γ and β parameters are
$\gamma \in (-30°, 125°)$
$\beta \in (-40°, 60°)$
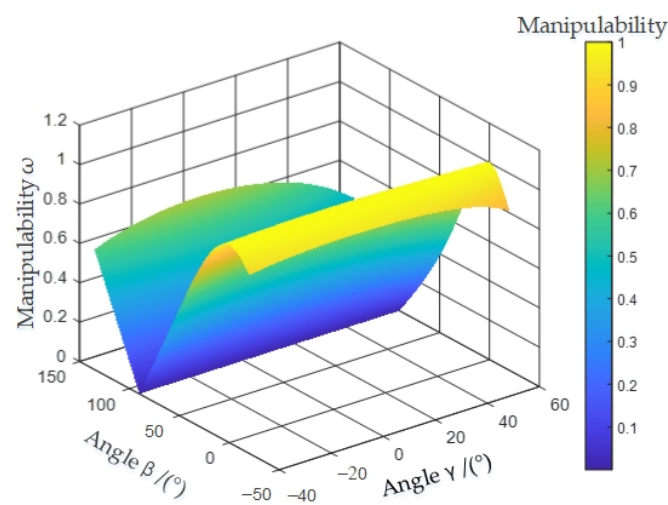In the above range of motion, the distribution of ω in the workspace is shown in Figure 4.

Figure 4. Distribution of ω values of the hip joint in the workspace.

Figure 4 shows the distribution of ω in the motion space, whose value ranges from 0.58 to 1.02, and the closer it is to the initial equilibrium position, the closer it is to 1. We concluded that the distribution of the manipulability ω value of the mechanism is between 0.58 and 1.02, and the variation is stable and continuous in the motion space.

To sum up, manipulability is one of the kinematic performance indices of the mechanism, and the closer the value of the index is to 1, the better the movement performance of the mechanism is. Figures 3 and 4 show that the movement performance of this spatial 8R mechanism is improved.

4. Analysis of Hip Joint Motion Laws

A simulation diagram of the hip joint is shown in Figure 5. The 3D model of the mechanism was established by SolidWorks, which was imported into ADAMS software, and the corresponding kinematic pairs and drive were added to establish the virtual prototype model. The input parameters of the model are the angle parameters of its two drives. ADAMS software simulation was used to analyze the motion performance of the mechanism through the estimation of variables such as velocity, acceleration, angular velocity and angular acceleration.

The coordinate system direction in ADAMS is as follows: the x axis is to the right along the line $R_{11}R_{21}$, the y axis faces vertically up, and the z axis is perpendicular to the xy plane. The drive is added to R_{11}, R_{21}, R_{18} and R_{28}. The forward flexion, posterior extension, abduction and adduction movements of the hip joint were simulated in ADAMS. The variations in the velocities and angular velocities of the moving platform for a single movement are shown in Figure 6.
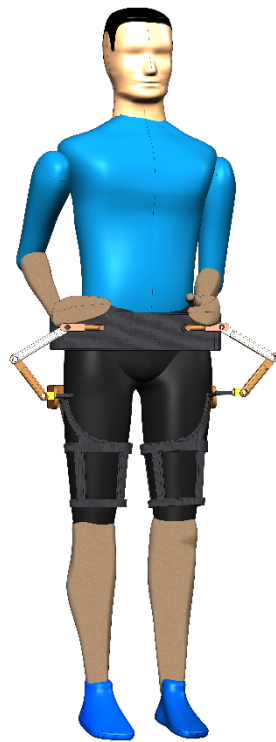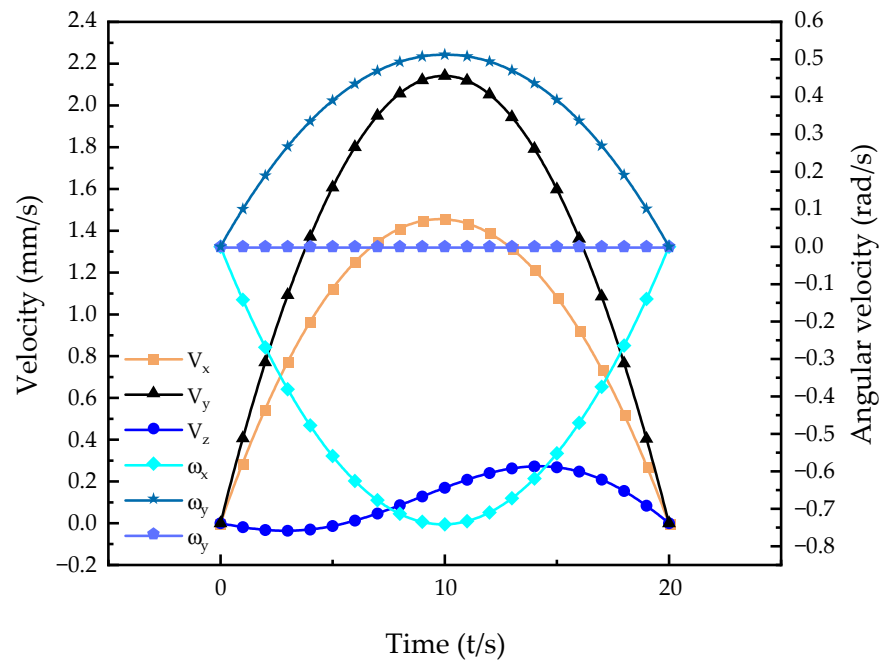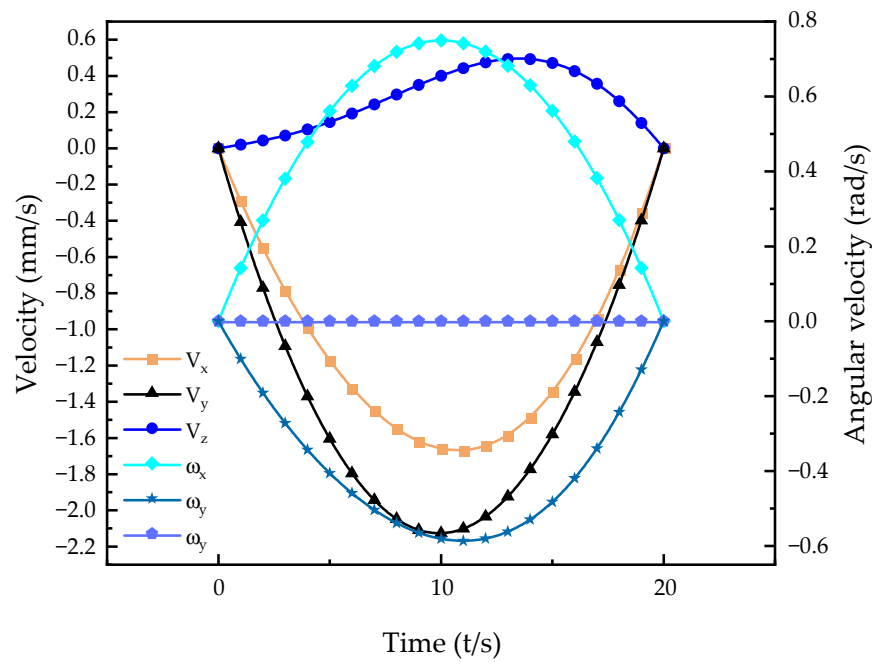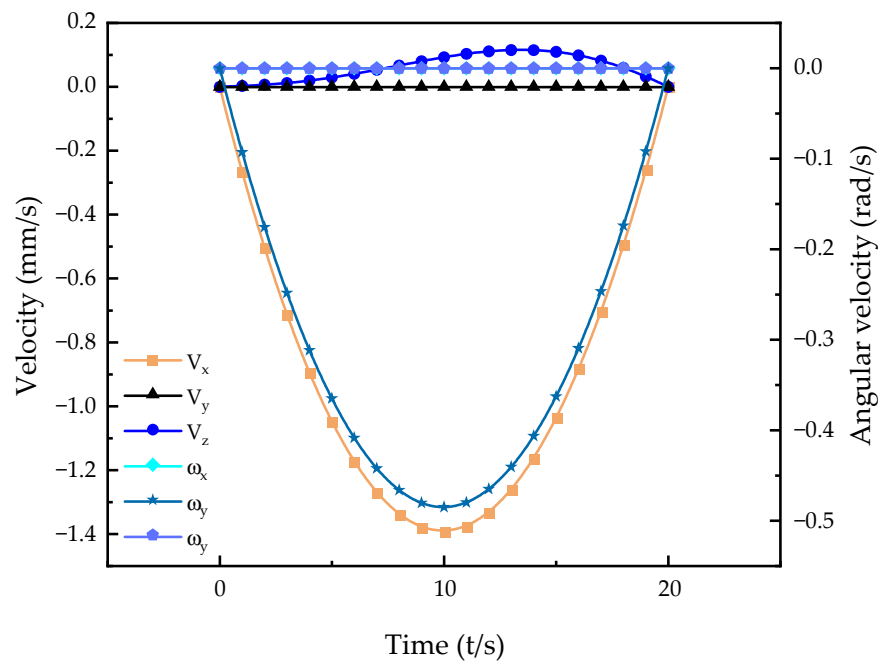
Figure 5. Wearable hip joint mechanism.

(**a**)

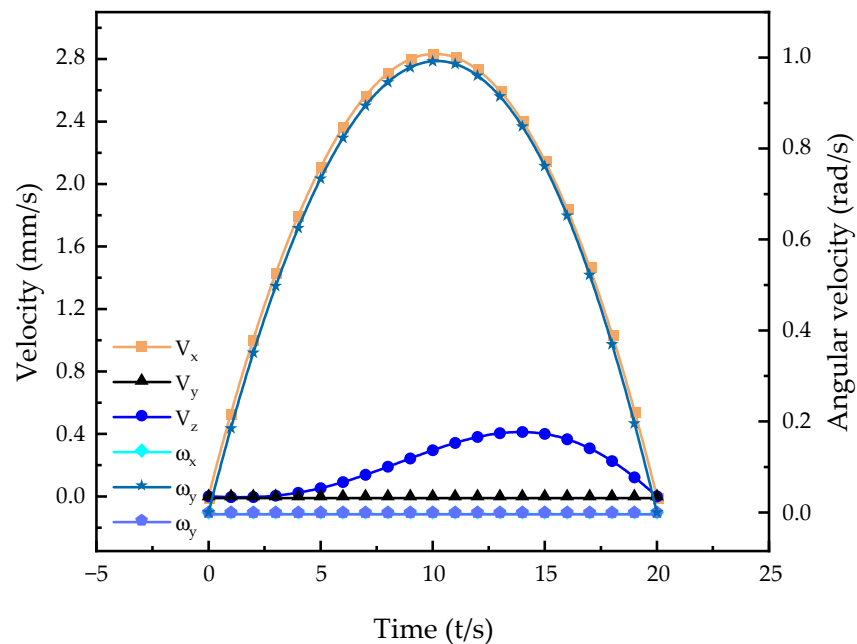**Figure 6.** *Cont*.

(**b**)

(**c**)

Figure 6. *Cont*.

(**d**)

Figure 6. Variations in the velocity and angular velocity of the moving platform *y* for a single movement. (**a**) Variations in the velocity and angular velocity of flexion motion. (**b**) Variations in the velocity and angular velocity of the extension motion. (**c**) Variations in the velocity and angular velocity of abduction motion. (**d**) Variations in the velocity and angular velocity of adduction motion.

As seen in Figure 5, the variation laws of various movements are relatively stable, and there is no break point, indicating that the movement performance of this mechanism is good and can be applied for hip rehabilitation. The coordinate system setting of the variation laws follow the coordinate system direction detailed in the first section, and around a certain axis, the inverse becomes positive, and the positive becomes negative. In the legend, V_x represents the velocity curve and ω_x represents the angular velocity curve. In forward flexion of the hip joint, the leg is lifted forward; thus, the velocity curve along the *y* axis changes considerably, and the velocity curve along the *x* axis changes as a joint linkage to ensure smoother forward flexion movement. There is no velocity in the *z* axis direction, so the velocity is 0. Since the forward flexion movement rotates around the *x* axis, the change in the angular velocity curve in the *x* axis direction is more obvious. The change in the angular velocity curve around the *y* axis is smaller than that around the *x* axis, and there is no rotation around the *z* axis; thus, the corresponding angular velocity curve is 0. The analysis of the velocity and angular velocity curves of other movements was carried out in the same manner. As seen in Figure 6, the movement of this mechanism can conform to the regular motion of the human hip joint, and therefore can be used to help patients recover.

5. Conclusions

Based on various hip joint rehabilitation mechanisms, a spatial 8R mechanism with two rotational degrees of freedom was proposed. The kinematic model of the mechanism was established, and the forward/inverse kinematics of the mechanism were analyzed using the D-H method of connecting rod parameters. Using the velocity Jacobian matrix and its condition number, the mechanism was found to be completely isotropic in the single movement of abduction and adduction, forward flexion and extension, and its dexterity was determined to be excellent. By analyzing the distribution pattern of the manipulability degree of the pose of the mechanism in the range of $-90° \sim 90°$, the singular configuration of the mechanism was found not to affect the normal motion of the mechanism.

According to the actual range of motion of various motion types of the human hip joint, the regular distribution of the maneuverability in the actual motion space of the hip joint is given, and its ω value was calculated to be distributed between 0.58 and 1.02, indicating that the mechanism has good motion characteristics. Kinematic simulation of the mechanism was carried out in ADAMS, and the velocity and angular velocity variations of the mechanism in different motion states were obtained. The kinematic performance of the mechanism was thus verified, proving the feasibility of using this mechanism for hip rehabilitation.

References

1. Shi, D.; Zhang, W.X.; Zhang, W.; Ding, X.L. A review on lower limb rehabilitation exoskeleton robots. *Chin. J. Mech. Eng.* **2019**, *32*, 74. [CrossRef]
2. Hendricks, H.T.; Limbeek, J.V.; Geurts, A.C.; Zwarts, M.J. Motor recovery after stroke: A systematic review of the literature. *Arch. Phys. Med. Rehab.* **2002**, *83*, 1629–1637. [CrossRef] [PubMed]
3. Cheng, L.; Chen, M.; Li, Z. Design and Control of a Wearable Hand Rehabilitation Robot. *IEEE Access.* **2018**, *6*, 74039–74050. [CrossRef]
4. Robert, B. Exoskeletons and robotic prosthetics: A review of recent developments. *Ind. Robot* **2009**, *36*, 5–18.
5. Glowinski, S.; Krzyzynski, T.; Bryndal, A.; Maciejewski, I. A kinematic model of a humanoid lower limb exoskeleton with hydraulic actuators. *Sensors* **2020**, *20*, 6116. [CrossRef] [PubMed]
6. Xiao, F.; Gao, Y.; Wang, Y.; Zhu, Y.; Zhao, J. Design and evaluation of a 7-DOF cable-driven upper limb exoskeleton. *J. Mech. Sci. Technol.* **2018**, *32*, 855–864. [CrossRef]
7. Chen, B.; Zi, B.; Qin, L.; Pan, Q. State-of-the-art research in robotic hip exoskeletons: A general review. *J. Orthop. Transl.* **2020**, *20*, 4–13. [CrossRef]
8. Pratt, J.; Carff, J.; Drakunov, S.; Goswami, A. Capture point: A step toward humanoid push recovery. In Proceedings of the 2006 6th IEEE-RAS International Conference on Humanoid Robots, Genova, Italy, 4–6 December 2006; pp. 200–207.
9. Hof, A.L.; Gazendam, M.G.J.; Sinke, W.E. The condition for dynamic stability. *J. Biomech.* **2005**, *38*, 1–8. [CrossRef]
10. Hof, A.L. The 'extrapolated center of mass' concept suggests a simple control of balance in walking. *Hum. Mov. Sci.* **2008**, *27*, 112–125. [CrossRef]
11. Gordon, K.E.; Ferris, D.P. Learning to walk with a robotic ankle exoskeleton. *J. Biomech.* **2007**, *40*, 2636–2644. [CrossRef]
12. Awad, L.N.; Bae, J.; O'donnell, K.; De Rossi, S.M.M.; Hendron, K.; Sloot, L.H.; Kudzia, P.; Allen, S.; Holt, K.G.; Ellis, T.D.; et al. A soft robotic exosuit improves walking in patients after stroke. *Sci. Transl. Med.* **2017**, *9*, eaai9084. [CrossRef] [PubMed]
13. Lee, J.; Huber, M.E.; Hogan, N. Applying hip stiffness with an exoskeleton to compensate gait kinematics. *IEEE Trans. Neural Syst. Rehabil. Eng.* **2021**, *29*, 2645–2654. [CrossRef] [PubMed]
14. Hsu, S.H.; Changcheng, C.; Lee, H.J.; Chen, C.T.L. Design and implementation of a robotic hip exoskeleton for gait rehabilitation. *Actuators* **2021**, *10*, 212. [CrossRef]
15. Zhang, W.; Zhang, W.; Shi, D.; Ding, X. Design of hip joint assistant asymmetric parallel mechanism and optimization of singularity-free workspace. *Mech. Mach. Theory* **2017**, *122*, 389–403. [CrossRef]
16. Zhang, W.; Zhang, S.; Ceccarelli, M.; Shi, D. Design and kinematic analysis of a novel metamorphic mechanism for lower limb rehabilitation. In *Advances in Reconfigurable Mechanisms and Robots*; First Online; Springer: Cham, Switzerland, 2015; pp. 545–558.
17. Rus, D.; Tolley, M.T. Design, fabrication and control of soft robots. *Nature* **2015**, *521*, 467–475. [CrossRef]
18. Karavas, N.; Kim, J.; Galiana, I.; Ding, Y.; Couture, A.; Eckert-Erdheim, A.; Walsh, C. Autonomous soft exosuit for hip extension assistance. In *Wearable Robotics: Challenges and Trends*; First Online; Springer: Cham, Switzerland, 2016; pp. 331–335.
19. Miller-Jackson, T.M.; Natividad, R.F.; Lim, D.Y.L.; Hernandez-Barraza, L.; Ambrose, J.W.; Yeow, R.C. A wearable soft robotic exoskeleton for hip flexion rehabilitation. *Front. Robot. AI* **2022**, *9*, 835237. [CrossRef]

20. Song, B.; Lee, D.; Park, S.Y.; Beak, Y. A novel method for designing motion profiles based on a fuzzy logic algorithm using the hip joint angles of a lower-limb exoskeleton robot. *Appl. Sci.* **2020**, *10*, 6852. [CrossRef]

21. Tseng, T.Y.; Lin, Y.J.; Hsu, W.C.; Lin, L.F.; Kuo, C.H. A novel reconfigurable gravity balancer for lower-limb rehabilitation with switchable hip/knee-only exercise. *J. Mech. Robot.-T ASME* **2017**, *9*, 041002. [CrossRef]

22. Pons, J.L. Rehabilitation Exoskeletal Robotics. *IEEE Eng. Med. Biol.* **2010**, *29*, 57–63. [CrossRef]

23. Ronsse, R.; Vitiello, N.; Lenzi, T.; van den Kieboom, J.; Carrozza, M.C.; Ijspeert, A.J. Human–robot synchrony: Flexible assistance using adaptive oscillators. *IEEE Trans. Biomed. Eng.* **2011**, *58*, 1001–1012. [CrossRef]

24. Ronsse, R.; Lenzi, T.; Vitiello, N.; Koopman, B.; van Asseldonk, E.; De Rossi, S.M.; van den Kieboom, J.; van der Kooij, H.; Carrozza, M.C.; Ijspeert, A.J. Oscillator-based assistance of cyclical movements: Model-based and model-free approaches. *Med. Biol. Eng. Comput.* **2011**, *49*, 1173–1185. [CrossRef]

25. Giovacchini, F.; Vannetti, F.; Fantozzi, M.; Cempini, M.; Cortese, M.; Lefber, D.; Vitiello, N. A light-weight active orthosis for hip movement assistance. *Robot. Auton. Syst.* **2015**, *73*, 123–134. [CrossRef]

26. Rodríguez-Fernández, A.; Lobo-Prat, J.; Font-Llagunes, J.M. Systematic review on wearable lower-limb exoskeletons for gait training in neuromuscular impairments. *J. Neuroeng. Rehabil.* **2021**, *18*, 22. [CrossRef] [PubMed]

27. Tan, K.; Koyama, S.; Sakurai, H.; Teranishi, T.; Kanada, Y.; Tanabe, S. Wearable robotic exoskeleton for gait reconstruction in patients with spinal cord injury: A literature review. *J. Orthop. Transl.* **2021**, *28*, 55–64. [CrossRef] [PubMed]

28. Schreiber, L.T.; Gosselin, C. Kinematically redundant planar parallel mechanisms: Kinematics, workspace and trajectory planning. *Mech. Mach. Theory* **2018**, *119*, 91–105. [CrossRef]

29. Gosselin, C.M.; Laliberté, T.; Veillette, A. Singularity-free kinematically redundant planar parallel mechanisms with unlimited rotational capability. *IEEE Trans. Robot.* **2015**, *31*, 457–467. [CrossRef]

30. Wang, J.; Gosselin, C.M. Kinematic analysis and singularity representation of spatial five-degree-of-freedom parallel mechanisms. *J. Robot. Syst.* **1997**, *14*, 851–869. [CrossRef]

31. Schappler, M.; Ortmaier, T. Dimensional synthesis of parallel robots: Unified kinematics and dynamics using full kinematic constraints. In Proceedings of the Sechste IFToMM D-A-CH Konferenz, Campus Technik Lienz, Tyrol, Austria, 27–28 February 2020.

32. Xie, F.; Liu, X.J.; Luo, X.; Wabenr, M. Mobility, singularity, and kinematics analyses of a novel spatial parallel mechanism. *J. Mech. Robot.-T ASME* **2016**, *8*, 061022. [CrossRef]